Engineering of optical and electrical properties of ZnO by non-equilibrium thermal processing: The role of zinc interstitials and zinc vacancies

Prucnal, S.; Wu, J.; Berencen, Y.; Liedke, M. O.; Wagner, A.; Liu, F.; Wang, M.; Rebohle, L.; Zhou, S.; Cai, H.; Skorupa, W.;

Originally published:

July 2017

Journal of Applied Physics 122(2017), 035303

DOI: https://doi.org/10.1063/1.4994796

Engineering of optical and electrical properties of ZnO by non-equilibrium thermal processing: the role of zinc interstitials and zinc vacancies

S. Prucnal[1,*], Jiada Wu[2], Y. Berencén[1], M. O. Liedke[3], A. Wagner[3], F. Liu[1], M. Wang[1], L. Rebohle[1], S. Zhou[1], Hua Cai[2], W. Skorupa[1]

[1]*Helmholtz-Zentrum Dresden-Rossendorf, Institute of Ion Beam Physics and Materials Research, Bautzner Landstraβe 400, D-01328 Dresden, Germany*

[2]*Shanghai Engineering Research Center of Ultra-Precision Optical Manufacturing, Department of Optical Science and Engineering, Fudan University, Shanghai 200433, China*

[3]*Helmholtz-Zentrum Dresden-Rossendorf, Institute of Radiation Physics, Bautzner Landstraβe 400, D-01328 Dresden, Germany*

Abstract

A controlled manipulation of defects in zinc oxide (ZnO) and the understanding of their electronic structure can be a key issue towards the fabrication of *p*-type ZnO. Zn vacancy (V_{Zn}), Zn interstitials (I_{Zn}) and O vacancy (V_O) are mainly native point defects determining the optoelectronic properties of ZnO. The electronic structure of these defects still remains controversial. Here, we experimentally demonstrate that the green emission in ZnO comes from V_{Zn}-related deep acceptor and V_{Zn}-V_O clusters, which is accompanied by the radiative transition between the triplet and the ground singlet state with the excited singlet state located above the CB minimum. Moreover, the I_{Zn} is identified to be a shallow donor in ZnO, being mainly responsible for the *n*-type conductivity of non-intentionally doped ZnO.

Keywords: ZnO, flash lamp annealing, defect engineering, photoluminescence.

*corresponding author: s.prucnal@hzdr.de

1. Introduction

Native point defects are the Achilles heel of ZnO. Most of them are donors being responsible for the *n*-type conductivity of ZnO even without intentional doping. It is well-known that annealing of ZnO in O-poor conditions leads to *n*-type layer formation while annealing in an O-rich atmosphere significantly reduces the electron concentration, and *p*-type conductivity is even observed under certain conditions [1-3]. The thermal treatment of ZnO in an O-poor ambient leads to the formation of Zn-interstitials (I_{Zn}) and O-vacancies (V_O). I_{Zn}^{+} (single charged), I_{Zn}^{++} (doubly charged) and I_{Zn}^{*} (neutral) are shallow donors with an energy level located between 30 and 220 meV below the bottom of the conduction band (CB) [4, 5]. Similar to I_{Zn}, V_O exists in neutral (V_O^{*}), single (V_O^{+}) and doubly charged states (V_O^{++}). According to theoretical models V_O is a deep donor with energy levels located at about 1 eV, 1.6 eV and 2.4 eV below the CB minimum, respectively [4]. Alternatively, annealing in an O_2 ambient promotes the formation of O-interstitials (I_O) and Zn-vacancies (V_{Zn}) which are deep acceptors [6]. Moreover, an O_2 ambient can oxidize the I_{Zn} centers and passivates the V_O defects [6]. The exact position of the energy level of I_O is controversial. I_O is a deep acceptor which can accept two electrons and has energy levels at 0.5 eV and 1.4 eV above the valence band (VB) maximum [7, 8]. Therefore, I_O itself should not participate in the *p*-type conductivity of ZnO at room temperature but can efficiently neutralize *n*-type defects like I_{Zn} and V_O [9].

The *p*-type conduction of ZnO annealed under O-rich condition can be explained by the formation of defect complexes where I_O is involved. In general, the origin of the *p*- and n-type conductivity in undoped ZnO still remains under discussion. Also, the electronic structure of defects is not yet fully understood. Fink has found, by *ab-initio* cluster calculations on the electronic structure of oxygen vacancies in ZnO, that if V_O is similar to F^{+}-like centers the first excited state should be located above the CB minimum [10]. A similar conclusion has

been reported by Sokol *et al.* [4]. Much earlier, Wei proposed that the emission observed from the F^+-like center is due to intra-defect transitions. [11]. Theoretically, the F^+-like center should exhibit a singlet to triplet transition but due to the fact that the first singlet level is deeply located at 1.36 eV above the CB minimum, such transitions have never been observed experimentally [4]. Fortunately, most of the point defects in ZnO are optically active and can be identified by standard photoluminescence (PL) and photoluminescence excitation (PLE) experiments. There is a general agreement that the blue-violet emission is likely originated from I_{Zn} while the green emission involves a radiative recombination between an electron at V_O and a hole from the VB or the radiative recombination of an electron from the CB and a hole at V_{Zn} [12]. Leiter *et al*. have proposed the singlet-to-triplet state model for V_O defects where the green luminescence (GL) involves the photoexcitation of the V_O center from the first excited singlet to the first excited triplet state and its radiative recombination to the ground triplet state [13]. A similar explanation for the GL was proposed by Kodama and Uchino, but V_O has to be considered as a very deep donor [14]. In fact, the energy level of V_O^{++} is about 2.4 eV below the CB and can fit to the model proposed by Kodama and Uchino. Moreover, they have also shown that the *n*-type conductivity in ZnO is caused by I_{Zn} and H-related centers. The role of defects and its interplay between the near-band gap emission (NBE) and the green luminescence as well as the scintillations between them have been studied in Ref. 6 using oxygen and hydrogen passivation.

In general, the formation energy for a certain defect type in ZnO depends on the relative position of the Fermi level [4]. During conventional annealing like rapid thermal annealing or furnace annealing, independently of the atmosphere, the Fermi level position continuously moves towards either the CB minimum or the VB maximum due to the concentration changes of either the donor- or acceptor-like defects, respectively. This continuously changes the defect formation energy during thermal treatment. Therefore, the control of defects during conventional annealing is challenging. In contrast, sub-second non-equilibrium thermal

processing offers a new alternative to control the defects in ZnO irrespective of the position of the Fermi level. Millisecond-range flash-lamp annealing (FLA) is one of the most promising annealing techniques for this purpose. It has been shown that the dopant and defect distribution in different crystalline solids can be well controlled by using this approach [15].

In this paper, we investigate the influence of the annealing atmosphere on the optical and electrical properties of ZnO films crystallized by sub-second non-equilibrium thermal processing. Applying millisecond range FLA and O-poor or O-rich atmosphere we have precise control on the concentration and the type of defects created in the annealed film, e.g. I_{Zn} which is difficult to control using standard equilibrium processing. The combination of optical, structural and electrical measurements allows us to clearly identify the role of certain defects in ZnO. Using temperature-dependent photoluminescence (TDPL) and PLE emission we experimentally confirm that the electronic structure of V_{Zn} in ZnO is that of a F^+-like center. We demonstrate that the green emission in ZnO is due to the photon absorption of the singlet state located above the CB minimum and the radiative triplet to singlet transition. Both V_{Zn} and V_{Zn}-V_O open volume defects are involved in the green emission. The *n*-type conductivity in ZnO is due to I_{Zn} which is a shallow donor. The origin of defects in ZnO is also investigated using positron annihilation spectroscopy (PAS). A phenomenological model of PL excitation and emission is presented.

2. Experimental section

ZnO layers were deposited on Si wafers using oxygen plasma-assisted reactive pulsed laser deposition (PLD). Prior to the ZnO deposition, the Si wafer was oxidized to form a 100 nm thick SiO_2 layer in order to avoid the influence of the Si substrate on the electrical measurements. A high-purity (99.999%) metallic zinc target was pulsed laser ablated in an oxygen plasma ignited by electron cyclotron resonance microwave discharge. The deposition temperature did not exceed 80 ^oC. A detailed description of the experimental equipment and

the deposition procedure has been reported in Refs. 16 and 17. The nominal thickness of the ZnO layers was about 150 nm. FLA in the millisecond range was applied in order to improve the crystallinity of the ZnO layers. Annealing was performed for 20 ms at a continuous flow of either N_2 or O_2 (99.999 purity). The energy density deposited onto the sample surface during the FLA process was in the range of 65 to 100 Jcm^{-2}. This corresponds to a surface temperature in the range of 700 to 1000 ^oC. Recently, the unique features of FLA were successfully utilized to control the dopant distribution in different semiconductors e.g. hyperdoped Si and ultra-doped Ge [18-20]. Further details about the FLA system can be found in Ref. 21.

Optical properties of the annealed samples were studied by TDPL and PLE. For the PL measurements, a He-Cd laser (325 nm, 20 mW power) and a Xe-lamp were used. The PL spectra were recorded using a monochromator (Jobin Yvon Triax 320) and a photomultiplier (Hamamatsu H7732-10). The PLE was performed using a Xe lamp for excitation. A closed-cycle Helium gas cooling system was used to perform the TDPL measurements in the temperature range of 10-300 K. The recrystallization of ZnO during the FLA process was confirmed by micro-Raman spectroscopy. The phonon spectra were determined by Raman spectroscopy in backscattering geometry in the range of 100 to 2500 cm^{-1} using a 325 nm He-Cd laser with a liquid-nitrogen cooled charge coupled device camera. Prior to the annealing, some samples were covered with an Al_2O_3 layer of 7 nm deposited by atomic layer deposition system at 150 ^oC in order to investigate the influence of the annealing temperature on the optical properties of the ZnO films. The influence of annealing conditions on the formation of open volume defects like V_{Zn} was determined by PAS using a mono-energetic positron beam accelerated in the energy range of 0.03-35keV. The annihilation gamma ray energy spectra were collected using Ge detector with an energy resolution of (1.09 ± 0.01) keV for the 511 keV line. Experimental details related to PAS are given in Refs. 22 and 23.

The conductivity type and carrier concentration of the annealed samples were determined by Hall Effect measurements using a commercial Lakeshore Hall System with van der Pauw geometry. Samples were measured in the temperature range of 5-300 K with a superconducting magnet. Gold electrodes were sputtered onto the four corners of the square-like samples. Silver glue was used to contact the wires to the gold electrodes. All contacts were confirmed to be ohmic by measuring current-voltage curves at different temperatures.

3. Results and discussion

3.a. Structural properties

Structural properties of the fabricated ZnO were investigated by resonant Raman and positron annihilation spectroscopies. Figure 1 shows resonant Raman spectra obtained from an as-deposited sample and samples annealed in O_2 or N_2 atmosphere. The peak position of the active phonon mode depends on the crystallinity, scattering geometry and composition of the investigated material. Optically active phonon modes in ZnO are longitudinal optical (LO) E_2^{high} (located at about 470 cm^{-1}), E_1 (583 cm^{-1}) and A_1 (574 cm^{-1}) phonon modes [17]. The E_1 and A_1 can only be observed together in randomly oriented polycrystalline ZnO. The appearing, of both the E_1 and the A_1 phonon modes depends on the orientation of the ZnO unit cell relative to the polarization of the incident laser beam in the backscattering geometry. The A_1(LO) phonon mode can be observed for a polarization field parallel to the c-axis of ZnO, while the E_1(LO) phonon mode is detectable when the polarization field is perpendicular to the c-axis. In our case the as-grown ZnO shows the A_1 (LO) phonon mode centered at 582 cm^{-1} and its overtones are located at 1164, and 1750 cm^{-1}. After annealing the A_1 (LO) phonon mode shifts to 570 cm^{-1} and its overtones are at 1142 and 1726 cm^{-1}. In annealed samples the 3^{th} order of the A_1 phonon mode overtone is already overlapped by the photoluminescence signal emitted by the ZnO film excited by the UV laser. Simultaneously, the full width at half maximum (FWHM) of the A_1 mode decreases from 26.3 cm^{-1} in the as-

deposited sample to 21.2 and 20.6 cm^{-1} after annealing in N_2 and O_2, respectively. This confirms the improvement of the ZnO crystallinity during ms-range FLA.

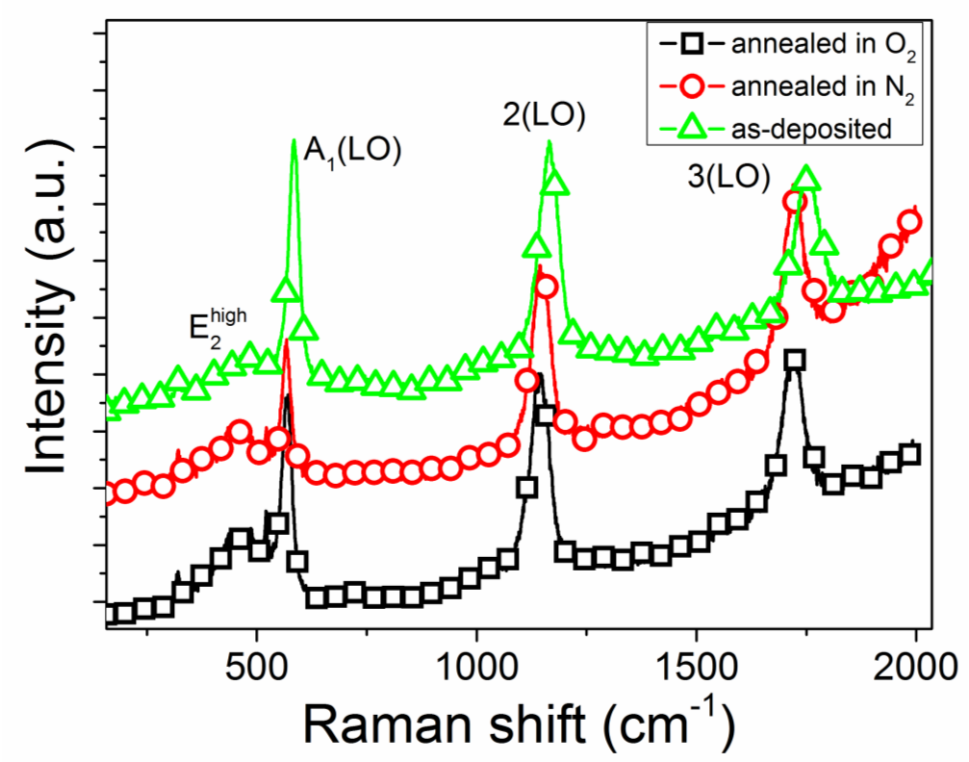

Figure 1. Resonant Raman spectra obtained from as-deposited and FLA treated ZnO for 20 ms in N_2 or O_2 atmosphere.

In order to clarify what kind of defects exist in ZnO after non-equilibrium ms-range FLA, Doppler broadening (DB)-PAS was performed (see Fig. 2). In general, DB-PAS can be used to determine defect transformations after different annealing conditions. PAS is most sensitive in detecting negatively charged and neutral open-volume defects where positrons can annihilate. In the case of ZnO the most common defects detected by PAS are V_{Zn} and their clusters. V_{Zn} in ZnO can be neutral or negatively charged (-1 or -2 state) [4]. Therefore, they can be effectively detected by PAS [23-25]. V_O in ZnO is a positively charged donor, and does not interact with positrons at room temperature. Fig. 2a shows the energy profile of the S parameter extracted from Doppler broadening spectra for the as-deposited sample and flash-lamp annealed ones in either N_2 or O_2 atmosphere for 20 ms at 80 Jcm^{-2}. The line shape of

parameter S depends on the Doppler broadening of the 511 keV annihilation line. The value of S is defined by the ratio of counts in the central region of the annihilation gamma peak to the total number of counts in the peak which is why the S-parameter characterizes the positron annihilation with low momentum electrons. In the case of good quality single crystalline material the S parameter is equal to 0.5 and it increases with increasing size of open volume defects e.g. by cluster formation [26]. The W parameter ("wing" or core annihilation parameter) is taken in the high-momentum region far from the center. The W parameter mainly describes the chemical environment of the investigated defect. The linear relationship between the S and W parameter indicates that only one type of defect exists in the investigated sample which traps positrons. In general, the detected positron energy can be recalculated from the depth profile using Makhov profiling [27]. The first 12-15 nm correspond to an annihilation energy below 1 keV, which basically represents positrons annihilating at the sample surface. The positron energy between 1 and 2 keV describes positrons anihilating at the depth up to 40-50 nm, thus in the bulk ZnO film. Positrons annihilating in a depth of more than 50 nm and approaching the SiO_2/ZnO interface (about 150 nm) are detected with a positron energy of about 3-4 keV. At first, independent of the treatment, the S parameter decreases with increasing positron energy due to a superposition of annihilation events at the sample surface and an enhancement of positron annihilation at defects in the nearest surface region. A small decrease of the S-parameter in the energy range up to 2 keV suggests a low positron diffusion length (L_+<20nm), thus relatively large defect concentration. After reaching the plateau at about 2 keV (about 40-50 nm from the surface) the S parameter starts to increase due to positrons attracted by the SiO_2 layer. The SiO_2 layer and the Si beneath are not within the scope of this paper. In order to have more information about the defect types in as-deposited and annealed samples the S-W plot was created. The linear behavior of a S-W plot implies a single type of open-volume defect as long as the measurement points lie on a line with measurements taken from reference sample, for

example, bulk ZnO [28]. In ZnO the annihilation centers are mainly related with V_{Zn} [28]. This is especially true for the as-grown film and a sample flashed in O_2 atmosphere, whereas N_2 annealing shows slightly shifted points at the positron energy range of 1.8-2.3 keV which corresponds to the bulk ZnO film. The former align with points from the deeper part of the samples, closer to the SiO_2 interface and possibly represents larger V_{Zn-O} complexes (neutral or positively charged) [29, 30]. Whereby, the latter comes to the same level for larger positron energy.

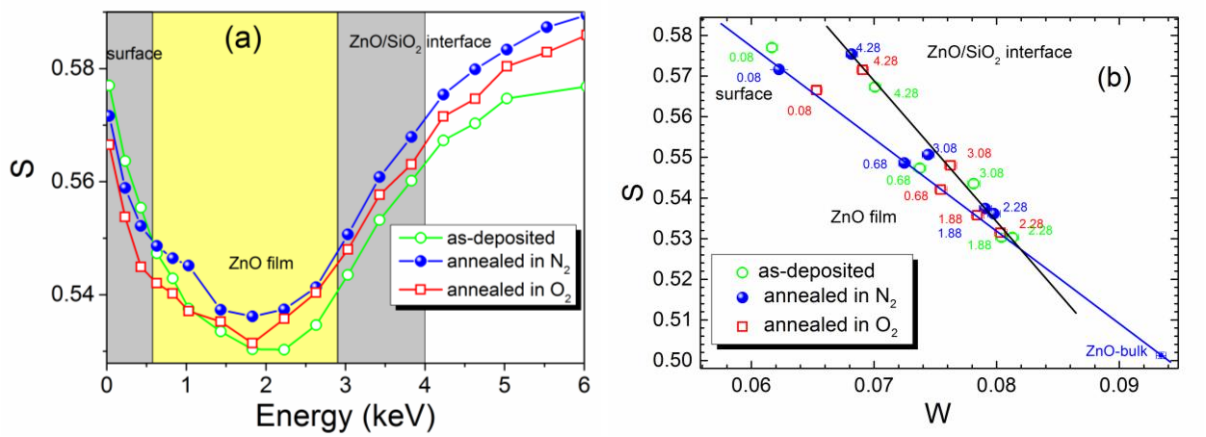

Figure 2. Calculated annihilation line parameter S as a function of positron energy E (a) and S-W plot showing different defect states as E-labels (b). Measurements were performed on as-deposited sample and samples annealed in oxygen or nitrogen atmosphere for 20 ms.

In our case the ZnO deposition was performed at room temperature. Therefore, the starting material is strongly disordered and annihilation of positrons takes place close to the implantation depth due to the low L_+. Trapping at the grain boundaries is the most probable origin of positron annihilation in ZnO. The S-W plot on Fig. 2b indicates that the annihilation centers are of V_{Zn} origin because of the linear relation with the ZnO bulk reference and in turn due to the fact that oxygen vacancies are not detectable with positrons (positive charge). After annealing in N_2 atmosphere, the S parameter decreases at first indicating an improvement of

the ZnO crystallinity close to the surface region and surface roughness. Later S increases which suggests an increase of the V_{Zn} concentration, and possibly the creation of V_{Zn-O} complexes (measurement points for E>2 keV lay off the line with ZnO-bulk). Most probably an increase of the V_{Zn} concentration is also accompanied by the formation of V_O being typical for ZnO films annealed in O-poor condition [27]. Thus, in the surface region V_{Zn} dominates, which turn into V_{Zn-O} complexes within the ZnO-film. Annealing in O_2 reduces the concentration of open volume defects within the first 50 nm (up to E=2 keV): not only V_O, which is expected, but also V_{Zn} and their complexes. Taking into account, the diffusion coefficient for O or N in ZnO at a temperature of about 1000 ^oC, 50 nm is the maximum thickness which can be modified by the annealing gases during a 20 ms FLA pulse. Moe Børseth *et al.* have investigated the influence of different annealing techniques on the defect formation in Li^+ implanted bulk ZnO [28]. They have shown that after FLA for 20 ms in air, most of the open volume defects are V_{Zn} clusters decorated by V_O. However, a pre-heating at 500 ^oC for 5 min was performed prior to FLA. The doped layer was about 2 μm thick which means that the annealing atmosphere did not play any significant role. Moreover, the pre-heating increases significantly the cooling time of the FLA sample which makes this process more similar to conventional rapid thermal annealing. In our case the ZnO film with a thickness of about 150 nm was heated up to 1000 ^oC within 10 ms while the total time for the sample at temperatures above 200 ^oC was shorter than 100 ms. Therefore, using ZnO thin films and FLA only, we can determine the influence of O-poor and O-rich conditions on the defect formation during strongly non-equilibrium thermal processing. The fact that after FLA the S-W plot shows linear behavior in the surface region independently of the annealing atmosphere implies that the concentration of V_{Zn} and V_O can be fully controlled. PAS results indicate that the annealing in N_2 ambient promotes the formation of the open volume V_{Zn}-V_O complex.

3.b. Optical properties of ZnO

Recently, Liu *et al.* have investigated the self-diffusion process of V_O in ZnO during conventional annealing [31]. Therein, it has been shown that O diffuses in ZnO via V_O and oxygen vacancies are mainly in the +2 charge state being shallow donors responsible for *n*-type conductivity of non-intentionally doped ZnO. On the contrary, most of the theoretical calculations show that V_O^{++} behaves as a deep donor. On the other hand, I_{Zn} is a shallow donor but it is difficult to achieve and stabilize I_{Zn} in ZnO. To verify the type and the role of defects formed during non-equilibrium ms-range FLA optical and electrical investigations were performed.

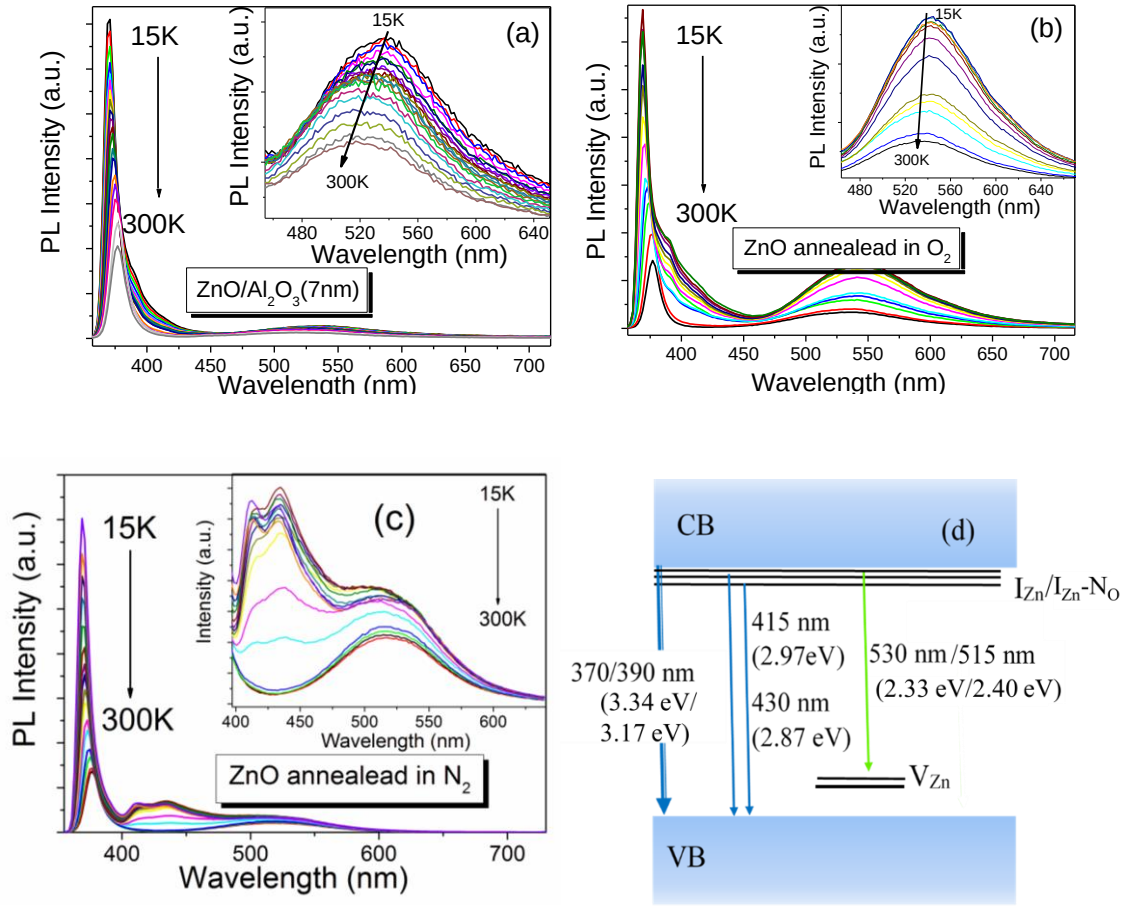

Figure 3. TDPL after FLA for 20 ms at 80 Jcm^{-2}. (a) prior to the annealing, the sample was covered by 7-nm-thick Al_2O_3 and the annealing was performed in N_2, (b) and (c) show TDPL spectra after annealing in O_2 and N_2 without capping layer, respectively. (d) shows the

schematic representation of the main radiative recombination mechanisms in FLA treated ZnO. The insets show the magnified visible part of the TDPL spectra.

Figure 3 shows the TDPL spectra obtained from the sample annealed with the Al_2O_3 capping layer (a) and samples annealed in O_2 and N_2 atmosphere without capping layer (b and c). In the case of the capped sample, the influence of the annealing atmosphere on the electrical and optical properties is expected to be negligible. Therefore, this sample can be used to investigate the impact of the non-equilibrium millisecond range FLA on the recrystallization mechanism and defect formation in ZnO. The sample annealed with the capping layer is *n*-type with an average carrier concentration in the order of 10^{17} cm^{-3}. The *n*-type conductivity is mainly due to native defects or unintentional contaminations, e.g. from the capping layer. The PL spectrum collected at 15 K shows strong near band-edge (NBE) emission peaking at 370 nm (3.34 eV) with a shoulder at 390 nm (3.17 eV) which is likely related to a neutral donor-bound exciton (D^0X), a free exciton (FX) and/or a donor-to-acceptor pair (DAP) (see Fig. 3a) [32, 33]. This peak shifts towards higher energy with decreasing the measurement temperature from 300 K to 15 K, and in turn the PL intensity gradually increases as the temperature decreases. Such a phenomenon is expected if excitons are involved in the luminescence process. After Gaussian deconvolution of the NBE emission and plotting the integrated PL intensity as a function of reciprocal temperature we have calculated the activation energy E_a according to the formula:

$$I(T) = \frac{I_0}{1+Ae^{-E_a/kT}}, \quad (1)$$

where $I(T)$ is the luminescence intensity at a given temperature T, I_0 is the initial intensity at 15 K, E_a is the activation energy, and A is a constant. The E_a obtained for 370 nm (3.34 eV) and 390 nm (3.17 eV) emissions are 62 meV and 72 meV, respectively.

The first value is in well agreement with the free exciton binding energy of ZnO (~60 meV). This indicates that the 370 nm (3.34eV) emission band is originated from FX, while the 390 nm (3.17 eV) emission peak comes from the D^0X transition [34]. Besides the UV part of the spectra the capped ZnO layer exhibits weak GL centered at about 520 nm (2.37 eV). This green emission is about 50 times weaker compared to the FX emission. To this day, there is a strong discussion in the community about the origin of the green emission in unintentionally doped ZnO. The green emission from ZnO is usually explained in terms of radiative recombination where V_O [35, 36] or V_{Zn} [37] are involved, as well as DAP, surface state defects and contaminations [35]. The interpretation of the visible part of the PL spectrum strongly depends on the fabrication method [38]. The annealing in O-poor conditions promotes the formation of I_{Zn} and V_O, while annealing in oxygen atmosphere favors the creation of I_O and V_{Zn}. Moreover, the green emission is often attributed to surface defects [39, 40] or transition metals like Cu [3]. For the case of the sample capped with Al_2O_3, O-poor conditions instead of O-rich ones must be considered. Simultaneously, the decomposition of ZnO and the out-diffusion of oxygen during annealing are limited by the capping layer. Additionally, the capping layer passivates surface state defects. If we take into account the position of the energy level of different defects in ZnO, the V_{Zn} and V_O seem to be the best candidates for the green emission. It was shown that V_{Zn} is a deep acceptor with an energy level located at about 0.8 eV above the VB maximum [38]. In contrast to V_{Zn}, the neutral V_O is a deep donor with an energy level about 0.9 eV below the CB minimum [41]. The GL in Al_2O_3 capped layer can originate from radiative recombination between: (i) either electrons in the CB or trapped by shallow donors and holes trapped by V_{Zn} or (ii) electrons trapped by V_O and holes in the VB. The red shift of the peak position with decreasing temperature suggests that holes from the VB and electrons from the CB are not directly involved in this emission (see inset in Fig. 3b). Thus, the most plausible explanation is that the GL originates from DAP, e.g. from a radiative recombination between electrons captured by shallow donors like

I_{Zn} and holes trapped at deep acceptor like V_{Zn} [5]. The TDPL spectra obtained from samples annealed without capping layer but at different annealing atmospheres significantly differ from each other (see Fig. 3b and 3c). During conventional annealing in O-rich atmosphere oxygen partially diffuses into ZnO and forms I_O defects. Moreover, the formation of V_{Zn} and the oxidation of V_O and I_{Zn} defects are also possible. The oxidation of shallow donors like I_{Zn} is proven by i) in contrast to Fig. 3c the absence of the low-temperature blue emission in the PL spectrum in Fig. 3b, and ii) the highly resistive nature of our samples. The room temperature carrier concentration calculated from Hall Effect data is below 10^{14} cm^{-3}. The sheet resistance measured at room temperature is in the range of several MΩ/sqr and increases up to 100 MΩ/sqr at 100 K. The position of the NBE peak coincides with the one coming from the sample annealed with capping layer, but the satellite PL emission at 390 nm (3.17 eV) originating from the D^0X is significantly quenched. The GL at RT is red-shifted by 15 nm compared to the sample annealed with capping layer and exhibits a much smaller red shift with decreasing temperature (see inset in Fig. 3b). The direct interpretation of PL spectra is always controversial since the electronic structure and the nature of defects strongly depend on the fabrication conditions of the ZnO films. Most probably, the GL observed here arises from a radiative recombination between electrons in the CB and holes captured by V_{Zn}.

Figure 3c shows the TDPL spectra obtained from samples annealed in nitrogen atmosphere where the formation of V_O and I_{Zn} is promoted. Therefore, after annealing in N_2 a highly conductive *n*-type layer is expected. In fact, samples annealed in N_2 show *n*-type behavior with an average carrier concentration above 2×10^{19} cm^{-3}. At RT the PL spectrum shows NBE emission at 375 nm (3.30 eV) and defect-related luminescence at 515 nm (2.40 eV). The GL observed from samples annealed in N_2 without capping layer can be assigned to the radiative recombination between electrons captured by V_O and holes in the VB. V_O is the most common defect in ZnO and has the lowest formation energy for annealing in O-poor conditions [38]. On the other hand, V_{Zn} can also be responsible for the GL. PAS data obtained

from sample annealed in N_2 indicates the existence of complex open volume defects like V_{Zn}-V_O and/or small $(V_{Zn})_x$ clusters (x<3). The presence of V_{Zn} in samples annealed in N_2 is possible because the formation energy of acceptor-type defects decreases with increasing Fermi level [38] and V_{Zn} is usually identified as a compensation center in *n*-type ZnO, which has often been detected by PAS [42]. Therefore, V_{Zn} are likely involved in the GL in samples annealed in N_2, and the model proposed by Kodama and Uchino can also be adapted for V_{Zn} [13]. More information about the excitation and emission from different defects can be extracted from PLE data (see section 3d). Taking into account equilibrium conditions for the sample processing, the types of defects present in ZnO are determined by formation energy and annealing atmosphere. However, the use of strongly non-equilibrium thermal processing for the crystallization of ZnO films has been considered here. In such a case the theoretical models cannot predict the formation energy for certain types of defects and the existence of I_{Zn} cannot be excluded.

At low temperature, the samples annealed in N_2 exhibit double blue peaks centered at 415 nm (2.98 eV) and 430 nm (2.87 eV). Most probably, the blue luminescence arises from the radiative recombination between electrons from shallow donors (I_{Zn}) or defect complex and holes in the VB. Although the formation energy of I_{Zn} is high, the existence of I_{Zn} in the sample annealed by FLA cannot be excluded. According to Sokol *et al.* the energy level of I_{Zn} is located about 220 meV below the CB which can explain the origin of the 430 nm (2.87 eV) emission but not that of the 415 nm (2.98 eV)band [4]. The energy level for a Zn-sublattice defect in ZnO was also estimated to be between 30 and 100 meV below the CB [43, 44] which would help to explain the origin of the second blue peak at 415 nm (2.98 eV). However, the I_{Zn} defects can be stabilized in ZnO in the form of complex defects e.g. with N on an O site (N_O) due to the low migration energy barrier of 0.55 eV. Look *et al* proposed that the main shallow donor in ZnO annealed in N_2 atmosphere is the I_{Zn}–N_O complex defect with an energy level located smaller than 100 meV below CB minimum [45]. Such a defect

complex can exist in our samples annealed in N_2 atmosphere and can be responsible for the 415 nm (2.98 eV) emission. The main radiative transitions observed in the PL spectra are shown in Fig. 3d.

3.c. Electrical properties of FLA treated ZnO

In order to shed light on the influence of the annealing parameters on the defect formation and electrical properties of the fabricated films, we have analyzed the kinetics of the temperature quenching of the PL emission together with the change of the electrical properties of ZnO as a function of temperature. Figure 4 shows the change of the integrated PL emission observed from I_{Zn} and V_{Zn} (a), isolated V_{Zn} (b) and the change of the sheet resistance as a function of the reciprocal temperature (open triangles). The PL spectra at different temperatures were deconvoluted to single peaks using Gaussian functions in order to deduce the activation energy associated with the different luminescent centers. The integrated PL intensity was plotted as a function of the reciprocal temperature and fitted using an Arrhenius plot given by formula (1). The activation energy calculated for the blue emission from ZnO films annealed in N_2 was found to be about 105 meV. The quenching kinetics of the I_{Zn} related emissions as a function of temperature follows the change of the sheet resistance. This also suggests that the I_{Zn} related defect complex is responsible for the *n*-type conductivity in ZnO and the most probably for the 415 nm (2.98 eV) emission. The observed green emission only slightly depends on the measurement temperature (in contrast to samples annealed with capping layer). The ionization energy extracted from the TDPL emission of V_{Zn} centers leads us to infer that the V_{Zn} is a deep acceptor and thus does not participate in the conduction mechanism of ZnO at room temperature. ZnO samples annealed in O_2 atmosphere show highly resistive behavior and the low temperature PL spectra only exhibit NBE and green emission (see Fig. 3b). Taking into account, the formation enthalpies of intrinsic point defects

in ZnO annealed in O-rich atmosphere the most energetically favorable process is the generation of V_{Zn} [4].

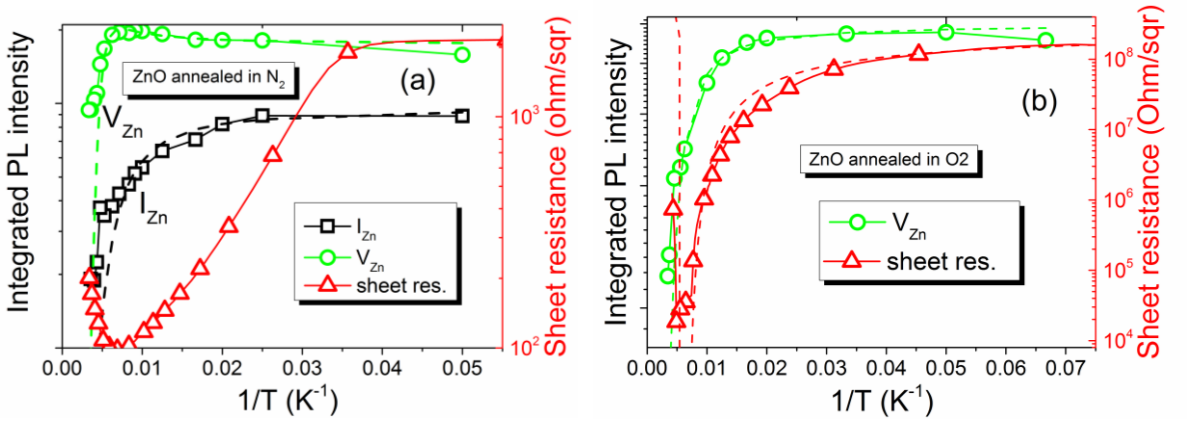

Figure 4. Integrated PL intensity and sheet resistance as a function of temperature measured for ZnO films annealed in N_2 ambient (a) and in O_2 ambient (b). The dashed lines are obtained by fitting the experimental data with an Arrhenius plot using formula (1).

In particular, V_{Zn} is a deep acceptor and has a minimum formation enthalpy when the Fermi level is located in the upper half of the band gap. Such conditions are fulfilled at the initial stage of the FLA process, and the existence of V_{Zn} defects is confirmed by PAS. Oxygen diffusion into the ZnO and oxidation of I_{Zn} take place even during our millisecond range non-equilibrium thermal processing. Therefore, the concentration of shallow donors decreases during annealing giving rise to the shift of the Fermi level towards the lower half of the band gap, where the lowest formation enthalpy is that for I_O [4]. In our samples, however, high concentrations of I_O are not expected since the annealing time is very short which significantly limits the amount of oxygen that can be accumulated in the ZnO film during ms-range annealing. This allows us to conclude that the main source of acceptors is V_{Zn}. This reasoning is also supported by the ionization energy extrapolated from TDPL and Hall Effect measurements and by PAS investigation. The minimum ionization energy of the V_{Zn} level deduced from the Arrhenius plot of the integrated PL intensity was found to be 720 meV,

while the activation energy of carriers calculated from the sheet resistance data was found to be 810 meV.

3.d. Phenomenological model of V_{Zn}

Photoluminescence excitation spectroscopy was carried out to investigate the electronic structure of intrinsic defects in ZnO. Figure 5a shows the PLE spectra of the green emission obtained from samples annealed in N_2 (open squares), O_2 (open triangles) and from bulk ZnO (open circles). After conventional annealing (e.g. 5 min at 900 ^oC in dry air, not shown here) all PLE spectra obtained for the emission peaking at 520 nm (2.37 eV) look similar to those obtained from bulk single crystalline ZnO (see open circles in Fig. 5a). In such a case, using PLE spectroscopy, we can only estimate the near-band edge and conclude that the excitation of the green emission with photon energy below the band gap is not possible. However, the observed PLE spectra, however, from flashed samples differ significantly.

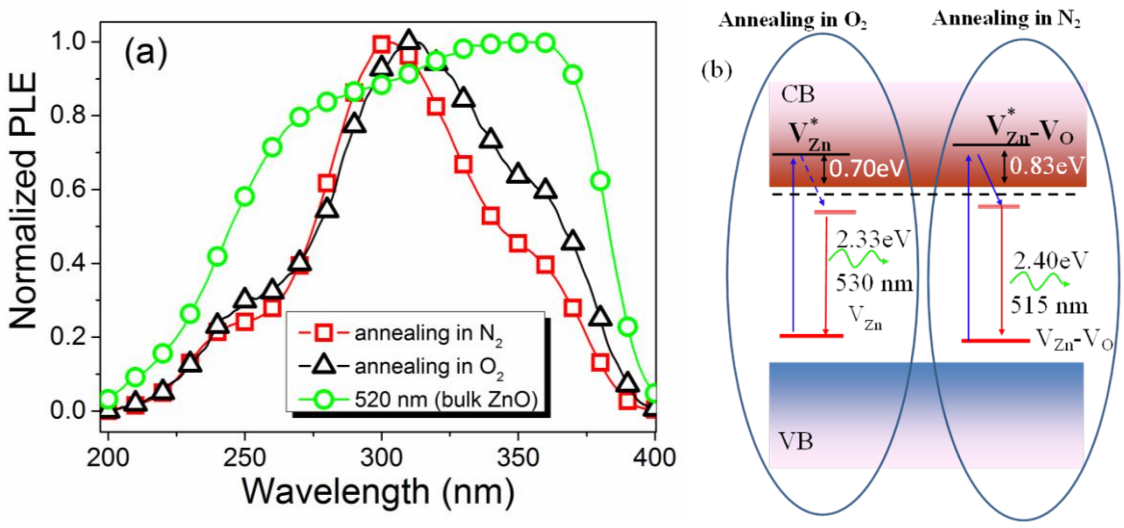

Figure 5. PLE spectra obtained from bulk single crystalline ZnO (open circles) and ZnO thin films annealed at different ambient (a). (b) shows the schematic representation of the electronic band structure of single V_{Zn} and V_{Zn}-V_O defects in ZnO, where the dashed line represents the energy level of shallow donors. Annealing was performed for 20 ms at a flash lamp energy density of 80 Jcm^{-2}.

Particularly, a well-defined peak at around 300 nm (4.12 eV) was recorded, which is opposite to the expected monotonic increase of the PLE intensity when the excitation energy approaches the energy of the band gap edge. Similar to the PL spectra the peak position depends on the annealing conditions. After annealing in N_2, the PLE peak for the green emission is located at 300 nm (4.12 eV) and red-shifted by 15 nm after annealing in O_2. The same shift was observed for the green emission in the PL spectra after changing the annealing conditions but the NBE peak position is the same for both samples. Moreover, PL spectra from samples annealed at different conditions using different excitation wavelengths between 240 nm (5.15 eV) and 370 nm (3.34 eV) were recorded. The PL peak position of the green emission was found to be independent of the excitation wavelengths (not shown here). This indeed proves that the first excited singlet level of the single-V_{Zn} and the V_{Zn}-V_O complex is located at around 0.7 eV and 0.83 eV above the CB minimum, respectively. The schematic representation of excitation and radiative transitions in ZnO containing either single-V_{Zn} or V_{Zn}-V_O complex defects after annealing in either O_2 or N_2, respectively, are shown in Fig. 5b. The NBE emission is not illustrated there. The direct observation of the electronic structure of excited V_{Zn} and V_{Zn}-V_O complex centers is possible because the millisecond range annealing allows us to control the type and the concentration of defects which is very challenging during conventional annealing processes.

4. Conclusions

We have experimentally verified the electronic structure of V_{Zn} in ZnO to be a F^+-like center. The first excited singlet level of V_{Zn} is located at about 0.7 eV above the CB minimum and V_{Zn} has been identified to be a deep acceptor in ZnO. The *n*-type conductivity in nonintentionally doped ZnO is ascribed to I_{zn} which is a shallow donor. The precise control of native defects in ZnO via millisecond range non-equilibrium thermal processing has allowed

us to significantly tune the conductivity of pristine ZnO samples from highly *n*-type to semi-insulating. The obtained results might be adapted to different oxides relevant for the industry like ITO, TiO_2, AZO.

5. Acknowledgement

This work was financially supported by Helmholtz-Gemeinschaft Deutscher Forschungszentren (VH-NG-713). YB would like to thank the Alexander-von-Humboldt foundation for providing a postdoctoral fellowship. The authors (FL and MW) were supported by China Scholarship Council. We would like to thank Ovidiu D. Gordan from TU Chemnitz, Germany, for Raman measurements.

6. References

1. V. Quemener, L. Vines, E. V. Monakhov, and B. G. Svensson, *Appl. Phys. Lett.* **100**, 112108 (2012).
2. U. Ilyas, R. S. Rawat, T. L. Tan, P. Lee, R. Chen, H. D. Sun, L. Fengji, and S. Zhang, *J. Appl. Phys.* **110**, 093522 (2011).
3. K. E. Knutsen, A. Galeckas, A. Zubiaga, F. Tuomisto, G. C. Farlow, B. G. Svensson, and A. Yu. Kuznetsov, *Phys. Rev. B* **86**, 121203(R) (2012).
4. A. A. Sokol, S. A. French, S. T. Bromley, C. R. A. Catlow, H. J. J. van Dam and P. Sherwood, *Faraday Discuss.* **134**, 267–282 (2007).
5. C. H. Ahn, Y. Y. Kim, D. C. Kim, S. K. Mohanta, and H. K. Cho, *J. Appl. Phys.* **105**, 013502 (2009).
6. J. Ji, A. M. Colosimo, W. Anwand, L. A. Boatner, A. Wagner, P. S. Stepanov, T. T. Trinh, M. O. Liedke, R. Krause-Rehberg, T. E. Cowan and F. A. Selim, *Sci. Rep.* **6**, 31238 (2016).

7. A. M. Gsiea, J.P. Goss, P. R. Briddon, R. M. Al-habashi, K. M. Etmimi, K. A. S. Marghani, World Acad. Sci. Eng. Technol. Int. J. Math. Comput. *Phys. Quantum Eng.*, **8**, 127 (2014).
8. A. F. Kohan, G. Ceder, D. Morgan, C. G. Van de Walle, *Phys. Rev. B* **61**, 15019 (2000).
9. R. Vidya, P. Ravindran, H. Fjellvåg, B. G. Svensson, E. Monakhov, M. Ganchenkova, and R. M. Nieminen, *Phys. Rev. B* **83**, 045206 (2011).
10. K. Fink, *Phys. Chem. Chem. Phys.*, **8**, 1482–1489 (2006).
11. W. F. Wei, *Phys. Rev. B* **15**, 2250 (1977).
12. J. Čížek, J. Valenta, P. Hruška, O. Melikhova, I. Procházka, M. Novotný, and J. Bulíř, *Appl. Phys. Lett.* **106**, 251902 (2015).
13. F. Leiter, H. Alves, A. Hofstaetter, D. Hofmann, and B. Meyer, *Phys. Status Solidi B* **226**, R4 (2001).
14. K. Kodama and T. Uchino, *J. Appl. Phys.* **111**, 093525 (2012).
15. S. Prucnal, L. Rebohle and W. Skorupa, Doping by Flash Lamp Annealing, *Mater. Sci. Semicond. Process.* **62**, 115-127 (2017).
16. K. Gao, W. Zhang, J. Sun, N. Xu, Z. F. Ying, Q. Li, J. Gan, and J. D. Wu, *J. Phys. Chem. C* **113**, 19139–19144 (2009).
17. S. Prucnal, K. Gao, S. Zhou, J. Wu, H. Cai, O. D. Gordan, D. R. T. Zahn, G. Larkin, M. Helm, and W. Skorupa, *Appl. Phys. Lett.* **105**, 221903 (2014).
18. L. Rebohle, S. Prucnal and W. Skorupa, *Semicond. Sci. Technol.* **31**, 103001 (2016).
19. S. Zhou, F. Liu, S. Prucnal, K. Gao, M. Khalid, C. Baehtz, M. Posselt, W. Skorupa and M. Helm, *Sci. Rep.* **5**, 8329 (2015).
20. S. Prucnal, F. Liu, M. Voelskow, L. Vines, L. Rebohle, D. Lang, Y. Berencén, S. Andric, R. Boettger, M. Helm, S. Zhou and W. Skorupa, *Sci. Rep.* **6**, 27643 (2016).
21. W. Skorupa, T. Gebel, R. A. Yankov, S. Paul, W. Lerch, D. F. Downey, and E. A. Arevalo, *J. Electrochem. Soc.* **152**, G436 (2005).

22. M. O. Liedke, W. Anwand, R. Bali, S. Cornelius, M. Butterling, T. T. Trinh, A. Wagner, S. Salamon, D. Walecki, A. Smekhova, H. Wende, and K. Potzger, *J. Appl. Phys.* **117**, 163908 (2015).

23. W. Anwand, G. Brauer, M. Butterling, H. R. Kissener, and A. Wagner, *Defect Diffus. Forum* **331**, 25 (2012).

24. J. Čížek, N. Žaludová, M. Vlach, S. Daniš, J. Kuriplach, I. Procházka, G. Brauer, W. Anwand, D. Grambole, W. Skorupa, R. Gemma, R. Kirchheim and A. Pundt, *J. Appl. Phys.* **103**, 053508 (2008).

25. Y. Dong, F. Tuomisto, B. G. Svensson, A. Yu. Kuznetsov and L. J. Brillson, *Phys. Rev. B* **81**, 081201 (2010).

26. L. Li, S. Prucnal, S. D. Yao, K. Potzger, , W. Anwand, A. Wagner, and S. Zhou, *Appl. Phys. Lett.* **98**, 222508 (2011).

27. J. C. Fan, C. Y. Zhu, S. Fung, Y. C. Zhong, K. S. Wong, Z. Xie, G. Brauer, W. Anwand, W. Skorupa, C. K. To, B. Yang, C. D. Beling and C. C. Ling, *J. Appl. Phys.* **106**, 073709 (2009).

28. T. Moe Børseth, F. Tuomisto, J. S. Christensen, W. Skorupa, E. V. Monakhov, B. G. Svensson, and A. Yu. Kuznetsov, *Phys. Rev. B* **74**, 161202(R) (2006).

29. M. Haseman, P. Saadatkia, D. J. Winarski, F. A. Selim, K. D. Leedy, S. Tetlak, D. C. Look, W. Anwand, A. Wagner, *J. Elec. Materi.* **45**, 6337–6345 (2016).

30. D. J. Winarski, W. Anwand, A. Wagner, P. Saadatkia, F. A. Selim, M. Allen, B. Wenner, K. Leedy, J. Allen, S. Tetlak and D. C. Look, *AIP Advances* **6**, 095004 (2016).

31. L. Liu, Z. Mei, A. Tang, A. Azarov, A. Kuznetsov, Q-K. Xue, and X. Du, *Phys. Rev. B* **93**, 235305 (2016).

32. E. Przeździecka, E. Kamińska, I. Pasternak, A. Piotrowska, J. Kossut, *Phys. Rev. B* **76**, 193303 (2007).

33. K. Samanta, A. K. Arora, S. Hussain, S. Chakravarty, R. S. Katiyar, *Curr. Appl. Phys.* **12**, 1381-1385 (2012).

34. B. K. Meyer, 1, H. Alves, D. M. Hofmann, W. Kriegseis, D. Forster, F. Bertram, J. Christen, A. Hoffmann, M. Straßburg, M. Dworzak, U. Haboeck, and A. V. Rodina, *Phys. Stat. Sol. (b)* **241**, 231– 260 (2004).

35. Y. Gong, T. Andelman, G. F. Neumark, S. O'Brien, I. L. Kuskovsky, *Nanoscale Res Lett.* **2**, 297–302 (2007).

36. S. A. Studenikin, N. Golego, M. Cocivera, *J. Appl. Phys.* **84**, 2287 (1998).

37. F. Tuomisto, K. Saarinen, D. C. Look, G.C. Farlow, *Phys. Rev. B* **72**, 085206 (2005).

38. A. Janotti and C. G. Van de Walle, *Rep. Prog. Phys.* **72**, 126501 (2009).

39. Y. H. Leung, X. Y. Chen, A. M. C. Ng, M. Y. Guo, F. Z. Liu, A. B. Djurišć, W. K. Chan, X. Q. Shi, M. A. Van Hove, *Appl. Surf. Sci.* **271**, 202– 209 (2013).

40. A. B. Djurišć, A. M. C. Ng, X. Y. Chen, *Progress in Quantum Electronics* **34**, 191 (2010).

41. P. A. Rodnyi and I. V. Khodyuk, *Optics and Spectroscopy* **111**, 776–785 (2011).

42. F. Tuomisto, K. Saarinen, D. C. Look, and G. C. Farlow *Phys. Rev.* B **72,** 085206 (2005).

43. A. R. Hutson *Phys. Rev.* **108** 222 (1957)

44. D. C. Look, J. W. Hemsky, and J. R. Sizelove, *Phys. Rev. Lett.* **82** 2552 (1999).

45. D. C. Look, G. C. Farlow, P. Reunchan, S. Limpijumnong, S. B. Zhang and K. Nordlund *Phys. Rev. Lett.* **95** 225502 (2005).